





# Dissecting Naturally Arising Amino Acid Substitutions at Position L452 of SARS-CoV-2 Spike

Toong Seng Tan,<sup>a,b</sup> Mako Toyoda,<sup>a,b</sup> Hirotaka Ode,<sup>c</sup> Godfrey Barabona,<sup>a</sup> Hiroshi Hamana,<sup>d</sup> Mizuki Kitamatsu,<sup>e</sup> Hiroyuki Kishi,<sup>d</sup> Chihiro Motozono,<sup>a,b</sup>  Yasumasa Iwatani,<sup>c</sup>  Takamasa Ueno<sup>a,b</sup>

<sup>a</sup>Joint Research Center for Human Retrovirus Infection, Kumamoto University, Kumamoto, Japan

<sup>b</sup>Graduate School of Medical Sciences, Kumamoto University, Kumamoto, Japan

<sup>c</sup>Clinical Research Center, National Hospital Organization Nagoya Medical Center, Nagoya, Aichi, Japan

<sup>d</sup>Department of Immunology, Faculty of Medicine, Academic Assembly, University of Toyama, Toyama, Japan

<sup>e</sup>Department of Applied Chemistry, Faculty of Science and Engineering, Kindai University, Osaka, Japan

**ABSTRACT** Mutations at spike protein L452 are recurrently observed in severe acute respiratory syndrome coronavirus 2 (SARS-CoV-2) variants of concern (VOC), including omicron lineages. It remains elusive how amino acid substitutions at L452 are selected in VOC. Here, we characterized all 19 possible mutations at this site and revealed that five mutants expressing the amino acids Q, K, H, M, and R gained greater fusogenicity and pseudovirus infectivity, whereas other mutants failed to maintain steady-state expression levels and/or pseudovirus infectivity. Moreover, the five mutants showed decreased sensitivity toward neutralization by vaccine-induced antisera and conferred escape from T cell recognition. Contrary to expectations, sequence data retrieved from the Global Initiative on Sharing All Influenza Data (GISAID) revealed that the naturally occurring L452 mutations were limited to Q, M, and R, all of which can arise from a single nucleotide change. Collectively, these findings highlight that the codon base change mutational barrier is a prerequisite for amino acid substitutions at L452, in addition to the phenotypic advantages of viral fitness and decreased sensitivity to host immunity.

**IMPORTANCE** In a span of less than 3 years since the declaration of the coronavirus pandemic, numerous SARS-CoV-2 variants of concern have emerged all around the globe, fueling a surge in the number of cases and deaths that caused severe strain on the health care system. A major concern is whether viral evolution eventually promotes greater fitness advantages, transmissibility, and immune escape. In this study, we addressed the differential effect of amino acid substitutions at a frequent mutation site, L452 of SARS-CoV-2 spike, on viral antigenic and immunological profiles and demonstrated how the virus evolves to select one amino acid over the others to ensure better viral infectivity and immune evasion. Identifying such virus mutation signatures could be crucial for the preparedness of future interventions to control COVID-19.

**KEYWORDS** SARS-CoV-2, L452, spike, substitution, fitness, coronavirus, mutational studies, spike protein

Since the emergence of severe acute respiratory syndrome coronavirus 2 (SARS-CoV-2) in the Wuhan province in China, this fast-evolving virus has acquired a significant number of mutations across its genome. As a result, many variants have surfaced in different parts of the world, such as the D614G variant, which first emerged in Europe during mid-2020 (1), and three major variants of concern (VOC) that emerged near the end of 2020, namely, the UK/alpha variant (B.1.1.7), the South Africa/beta variant (B.1.351), and the Brazil/gamma variant (P.1) (2–4). In the middle of 2021, the world was plagued with the

**Editor** Mark T. Heise, University of North Carolina at Chapel Hill

**Copyright** © 2022 American Society for Microbiology. All Rights Reserved.

Address correspondence to Takamasa Ueno, uenotaka@kumamoto-u.ac.jp.

The authors declare no conflict of interest.

**Received** 29 July 2022

**Accepted** 25 September 2022

**Published** 10 October 2022

fast-spreading delta variant (B.1.617.2) (5) before it was replaced with the currently circulating VOC, the omicron variant (B.1.1.529) (6).

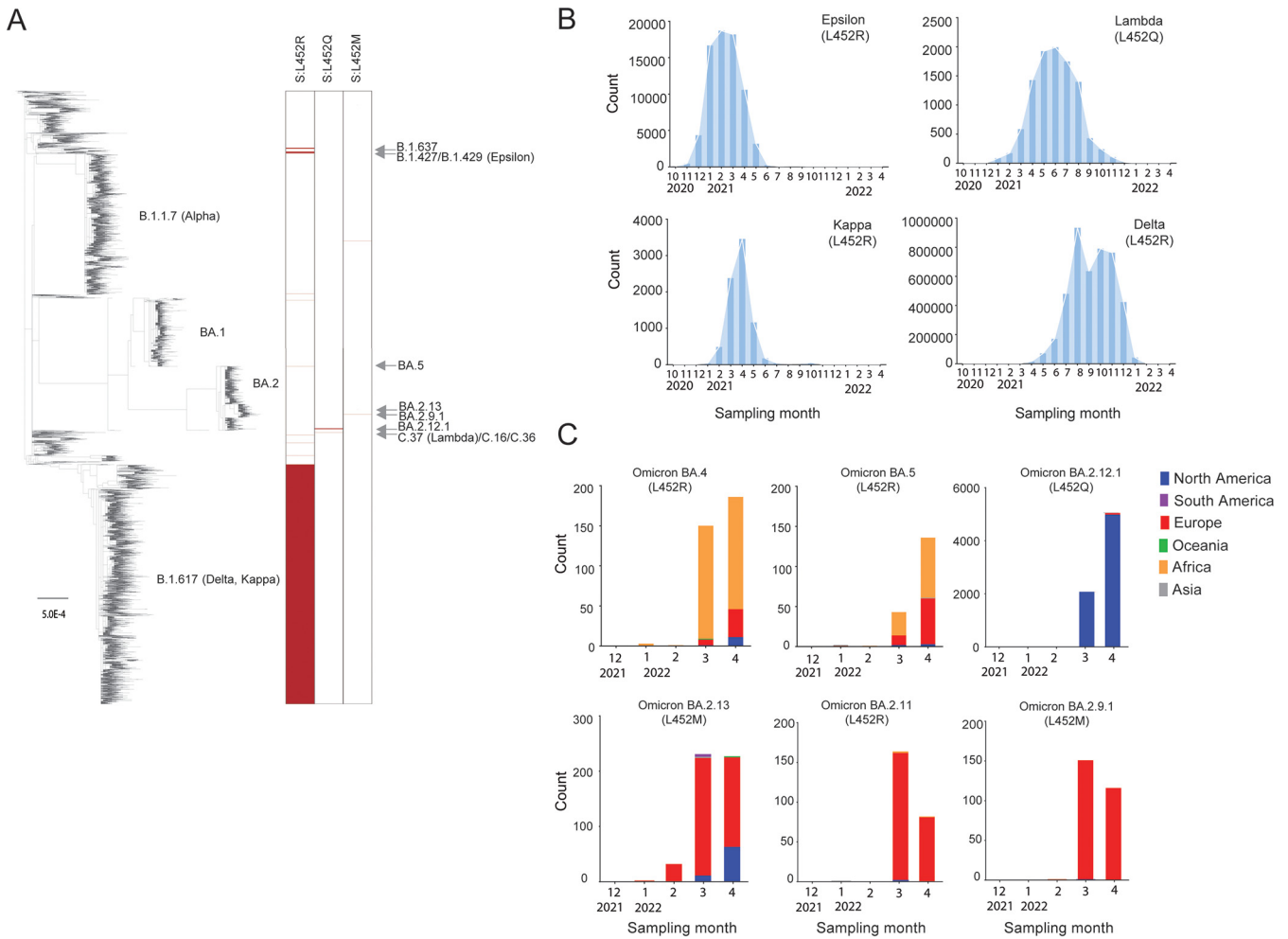
The L452R mutation located within the receptor-binding domain (RBD) of the SARS-CoV-2 spike, first garnered attention during multiple outbreaks in California, United States, where a sharp rise of sequences harboring L452R was detected from September 2020 to January 2021 in the genome sequences deposited in the Global Initiative on Sharing All Influenza Data (GISAID) (7–9). Prior to that, mink-associated L452M variant was found in several mink farms in the Netherlands, where few cases of two-way transmission from human to mink and back to human were reported (10–12). Thereafter, similar L452-associated mutations, including L452Q-harboring C.37 lineage (lambda variant) (13) and L452R-harboring B.1.617.1/2 lineage (kappa and delta variants) (14) and A.27 lineage (15) were also reported. Several reports suggested that L452R contributed to the enhanced infectivity and reduced susceptibility to antibody neutralization that is observed in these SARS-CoV-2 lineages (8, 13, 16–19). In addition, the L452 is located within a 9-mer immunodominant cytotoxic T lymphocyte (CTL) epitope presented by HLA-A\*24:02 (<sub>448</sub>NYNYLYRLF<sub>456</sub>) (20–22), where L452R mutation confers escape from HLA-A\*24:02-restricted CTL recognition (23).

In this study, we devised to clarify why certain amino acids are preferentially selected over the others in the light of global mutation landscape of the L452 variants. We constructed a panel of L452 spike mutants substituted with all 19 canonical amino acids and investigated their phenotypical, functional and immunological impacts. Our study showed that single nucleotide accessible mutation (SNAM) is the prerequisite factor for amino acid selection in L452 mutation, which was ultimately shaped by viral fitness and sensitivity to host immunity.

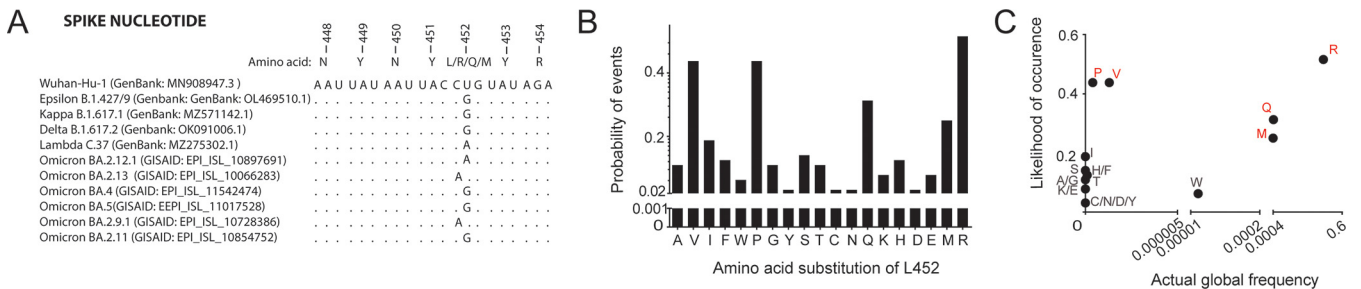
## RESULTS

**Recurrent mutations at spike L452 in multiple lineages of SARS-CoV-2.** We constructed a phylogenetic tree based on major SARS-CoV-2 genotypes ( $n = 25,796$ ) extracted from GISAID databases as of 27 April 2022, where 10,113 of them (~39%) had the spike L452 substituted with either arginine (R), glutamine (Q), or methionine (M) (Fig. 1A). These strains were derived from multiple SARS-CoV-2 lineages isolated from over 35 countries across all six continents. When we analyzed the timeline of the emergence of SARS-CoV-2 variants of interest (VOI) or VOC, the L452 mutation was first reported in VOI Epsilon (L452R) expanded in California (17, 24) from November 2020 but peaked in March 2021 (Fig. 1B). Following that, VOI Lambda (L452Q), which was first reported in Peru (25) in December 2020, then went on to spread in the South America countries in the first half of 2021 before declining (Fig. 1B). Meanwhile, VOI Kappa (L452R) (14), and VOC Delta (L452R) (5) were identified in India in October 2020. VOC Delta ended up becoming the predominant variant circulating globally from the second half of 2021 before it was replaced by the omicron variant in November 2021 (Fig. 1B). Very recently, several lineages of omicron acquired additional mutations, including at position L452. These omicron subvariants have since been assigned by the World Health Organization (WHO) to the newly added category, termed omicron VOC lineages under monitoring (VOC-LUMs) (26). We collected the metadata of deposited sequences from GISAID and depicted the trend of these omicron VOC-LUMs in different continents across the globe from January until the end of April 2022 (Fig. 1C). During this period, the BA.4 and BA.5 variants (harboring L452R) dominated South Africa, while the BA.2.12.1 subvariant (harboring L452Q), which was first detected in New York, outcompeted the BA.2 variant to become the dominant subvariant all over the United States. Other VOC-LUMs, including BA.2.13 (harboring L452M), BA.2.9.1 (harboring L452M), and BA.2.11 (harboring L452R), were showing signs of expansion in Europe (27) (Fig. 1C). The global emergence of L452 mutations in multiple lineages of SARS-CoV-2 demonstrated a pattern of convergent evolution, suggesting a common beneficial trait for the emerging variants.

**Codon base change as a genetic barrier in the global occurrences of spike L452 mutation.** When we aligned the part of nucleotide sequences encompassing the region encoding position 452, we noticed that all nonsynonymous mutations at this



site in epsilon, delta, kappa, lambda, and the omicron VOC-LUMs resulted from a single nucleotide substitution within the CUG codon of the ancestral Wuhan-Hu-1 strain (Fig. 2A). In light of this, we calculated the probability of occurrences of each canonical amino acid substitution at this position when leucine encoded by CUG as the



prototype sequence, with the single ( $P = 0.25$ ), doublet ( $P = 0.0625$ ), or triplet ( $P = 0.0156$ ) substitution required to achieve a nonsynonymous mutation and the number of codons available for a particular amino acid. We used a neutral model of codon substitution probability estimation without weighing in on codon preferences or the mutation rate of the virus because SARS-CoV-2 is known to have a relatively low codon usage bias (28). The analysis showed that the substitutions with the highest probability of occurrence are L452R ( $P = 0.516$ ), followed by L452P and L452V (both  $P = 0.438$ ), L452Q ( $P = 0.313$ ), and L452M ( $P = 0.25$ ) (Fig. 2B), suggesting that newly arising variants (e.g., Q, M, and R) have a low genetic barrier toward the codon change at this position. This is in agreement with a prior global mutational analysis study of SARS-CoV-2, which demonstrated that SNAMs are present at much higher frequencies (29). However, some exceptions on the basis of selection pressure exist, for instance, certain L452 mutations despite having a lower genetic barrier (e.g., P and V) showed very low global frequency (Fig. 2C), suggesting phenotypic constraints in these mutations.

#### Changes in spike-mediated fusion and pseudovirus entry by L452 mutations.

By constructing a set of spike mutants substituted with 19 different canonical amino acids at position L452, we first tested the effect on the steady-state expression of the spike protein in 293T cells after transfection of spike-encoding plasmids. Immunoblot analyses showed that wild-type (WT) spike was detected both in the full-length (180 kDa) and the cleaved forms (90 kDa) (Fig. 3A). While 14 of 19 mutants showed expression levels comparable to that of WT for both the full-length and cleaved forms, expression of the cleaved form was substantially reduced in L452 mutations to P and C and moderately reduced in I, N, and D mutations. However, the expression level of the full-length forms was not reduced in these mutants, suggesting either inefficient cleavage by a host protease or instability of the cleaved forms following the mutations (Fig. 3A). The introduction of P and C mutations at position 452 may trigger conformational defect of the spike protein (30, 31) and may lead to altered protein processing by host proteases and/or enhanced degradation by host machinery (32).

We then prepared lentiviral particles pseudotyped with the spike mutants. In addition to the P and C mutations, L452 mutations to I, N, and D showed substantial impairment both in spike incorporation into the nascent virions (Fig. 3A) and in production of the progeny viral particles (Fig. 3B), most likely reflecting the reduced cleaved form of the spike protein observed in these mutants. The rest of the mutants showed spike incorporation to virions and the subsequent production of progeny virions at levels comparable to WT. Of note, although the L452 mutations to I, P, and C exhibited substantial impairment in the incorporation of spike into lentiviral particles, I and L are considered to have relatively similar chemical properties compared to the side chain moieties of P and C (Fig. 3A).

Next, we tested the effect of the mutations on the infectivity of pseudotyped viral particles toward 293T target cells transiently expressing human ACE2 receptor and serine protease TMPRSS2 (33). As expected from these data, the L452 mutations to P, C, I, and D diminished the infectivity potential of the pseudoviruses to less than 50% of the WT level (Fig. 3C). The L452 mutations to Q, K, H, M, and R showed a >2-fold increase in infectivity compared to the WT (Fig. 3C), indicating that not only naturally arising mutants (i.e., Q, M, and R) but also naturally absent mutants (i.e., K and H) can enhance infectivity. In contrast, compared to WT, the L452 mutations to A, V, F, W, G, Y, S, T, and E retained infectivity (within a 2-fold increase) (Fig. 3C). Because L452-M, -Q, and -R mutations recently appeared in multiple lineages derived from omicron BA.2 (Fig. 1C), we tested the effect of these naturally arising mutations on pseudovirus infectivity in the context of the omicron spike backbone. Notably, we observed that introduction of M, Q, and R mutations to the parental BA.2 spike demonstrated a pronounced effect on enhancing infectivity (3- to 5-fold) (Fig. 3D), suggesting a common role of L452 mutations in the context of multiple variant lineages.

Fusogenicity between spike and host membranes via its interaction with the ACE2 receptor is known to be important for SARS-CoV-2 infectivity and transmissibility (34).

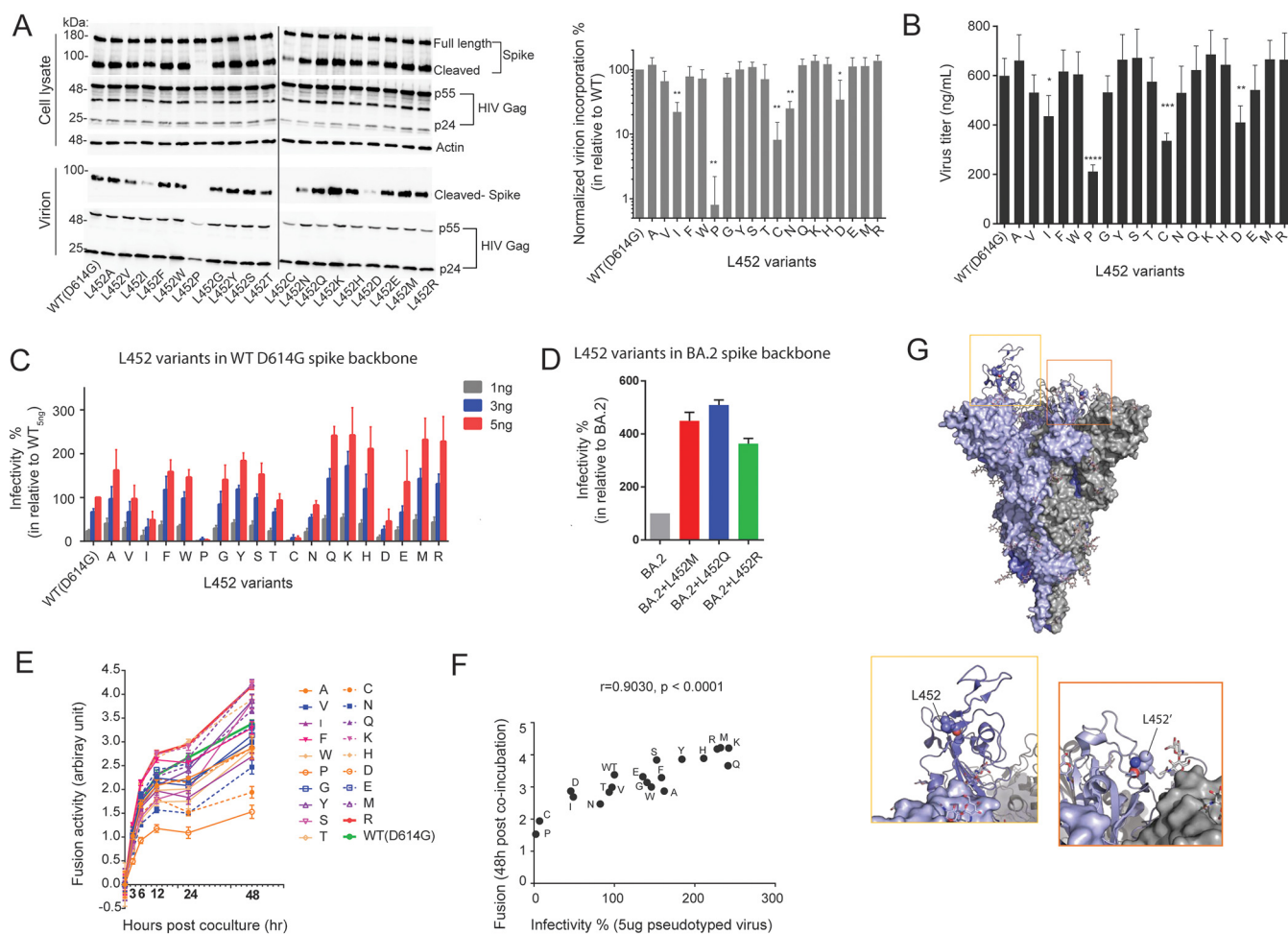


**FIG 3** Biochemical and virological characterization of spike L452 variants. (A) Immunoblots showing total cellular expression and virion incorporation of spike L452 mutants in producer cell and virion (left panel). The spike incorporation level was quantified and normalized to p24 Gag levels and is expressed relative to the WT in three independent replicates (right panel). Statistical significance was determined by one-way ANOVA with multiple-comparison tests (\*,  $P < 0.05$ ; \*\*,  $P < 0.01$ ; \*\*\*,  $P < 0.001$ ). (B) Titers (ng/mL) of pseudoviruses collected from the culture supernatant at 48 h posttransfection. (C) Infectivity of reporter lentiviruses pseudotyped by SARS-CoV-2 spike L452-mutants and WT D614G. The indicated titers of pseudoviruses (1, 3, and 5 ng) were exposed to 293T cells expressing ACE2 and TMPRSS2. The amount of pseudoviruses successfully infected into target cells was determined from the luciferase activity, and the relative infectivity is expressed as the percentage normalized to the WT (infection at 5 ng). (D) Infectivity of reporter lentiviruses pseudotyped with SARS-CoV-2 spike and its L452 mutants (infection at 5 ng). (E) Fusion formation between the spike-expressing cells and ACE2-TMPRSS2-expressing cells was continuously monitored at intervals of 3, 6, 12, 24, and 48 h. The fusion activity was expressed relative to WT at 3 h after cocultivation. (F) Correlation between infectivity of pseudoviruses (infection at 5 ng) and cell-to-cell fusion activity (at 48 h). The statistical significance was determined by using the Pearson's correlation coefficient test. (G) Structure of SARS-CoV-2 spike trimer with single RBD up-conformation (PDB 7KRR). Each protomer is differently colored. The L452 residues are shown as spheres, while glycans are indicated as sticks. In the RBD with the up-conformation, the L452 residue is exposed (yellow box). In contrast, in the RBD with the down-conformation, the L452 residue is buried at the interface with the NTD of another protomer (orange box). The data shown are means  $\pm$  the SD of triplicate determinations.

We therefore analyzed the spike-mediated cell-to-cell fusion using a dual-split reporter protein system (DSP) (35). Time course experiments showed that the cell-to-cell fusion commenced immediately after initiating coculture of spike and ACE2/TMPRSS2-expressing cells and continued for at least 48 h. The L452 substitutions to amino acid residues harboring basic side chains (i.e., K, R, and H) exhibited cell-to-cell fusion most efficiently (Fig. 3E). In contrast, fusogenicity of the L452P mutant was the lowest, most likely because of impaired cleavage of the spike protein in the cells (Fig. 3A). Of interest, the L452D mutant exhibited only approximately 15% reduction in fusion activity compared to WT; although it showed much more impairment in the virion incorporation of the spike protein (Fig. 3A) and in infectivity of the pseudovirus particles (Fig. 3C). It remains unclear whether incorporation of the L452D spike is similarly abrogated in authentic SARS-CoV-2. Overall, the fusion activity and the infectivity of pseudoviruses were well correlated ( $r = 0.9030$ ,  $P < 0.0001$ ) (Fig. 3F), confirming the importance of



**TABLE 1** Vaccinated donors in this study

Donor no.	Sex	Age (yrs)	No. of doses	Doses			Time since last shot (days)	History of COVID-19	pNT50 <sup>a</sup> against:	
				1	2	3			WT <sup>b</sup>	BA.2 <sup>c</sup>
1	F	18	2	BNT162b2	BNT162b2	NA <sup>d</sup>	21	No	3685.391	NA
2	F	24	2	BNT162b2	BNT162b2	NA	22	No	858.9506	NA
3	F	25	2	BNT162b2	BNT162b2	NA	23	No	585.8983	NA
4	M	23	2	BNT162b2	BNT162b2	NA	22	No	824.0571	NA
5	M	34	2	BNT162b2	BNT162b2	NA	14	No	779.7973	NA
6	M	55	2	BNT162b2	BNT162b2	NA	14	No	1037.38	NA
7	M	35	2	BNT162b2	BNT162b2	NA	14	No	1821.565	NA
8	M	33	2	BNT162b2	BNT162b2	NA	13	No	506.6158	NA
9	F	57	2	BNT162b2	BNT162b2	NA	10	No	1504.086	NA
10	M	23	3	BNT162b2	BNT162b2	mRNA-1273	44	No	NA	525.8267
11	F	29	3	BNT162b2	BNT162b2	mRNA-1273	40	No	NA	228.7586
12	F	24	3	BNT162b2	BNT162b2	mRNA-1273	42	No	NA	167.915
13	M	22	3	BNT162b2	BNT162b2	mRNA-1273	42	No	NA	336.4254
14	F	23	3	BNT162b2	BNT162b2	mRNA-1273	43	No	NA	201.9978
15	M	23	3	BNT162b2	BNT162b2	mRNA-1273	44	No	NA	155.8458
16	M	56	3	BNT162b2	BNT162b2	mRNA-1273	24	No	NA	191.1671
17	M	39	3	BNT162b2	BNT162b2	mRNA-1273	24	No	NA	133.8658
18	F	67	3	BNT162b2	BNT162b2	BNT162b2	15	No	NA	124.8006

<sup>a</sup>pNT50, pseudovirus 50% neutralization titer (serum dilution).

<sup>b</sup>WT, wild-type D614G (B.1 lineage).

<sup>c</sup>BA.2, Omicron BA.2 (B.1.1.529 lineage).

<sup>d</sup>NA, not applicable.

fusogenicity between spike and host membrane via its interaction with the ACE2 receptor in the viral entry to the target cells.

Previously reported cryo-electron microscopy structure of full-length spike trimer shows that the L452 amino acid residue in RBD at down conformation is buried at the interface with the N-terminal domain (NTD) of another protomer (PDB 7KRR) (36) (Fig. 3G). It was also demonstrated that the delta variant bearing spike L452R has an up-conformation more frequently than that of D614G variant (37). In parallel, our mutagenesis study demonstrated that amino acids with positive charge (e.g., R, K, and H) and/or long side chain (e.g., R, K, Q, and M) at position 452 of SARS-CoV-2 spike have a positive effect on viral entry. Hence, it is electrostatic repulsion or steric hindrance of the 452nd residue with its neighboring NTD that may induce RBD up-conformation which is more accessible to ACE2 entry receptor (37).

**Changes in immune recognition of spike proteins by L452 mutations.** We obtained a panel of antisera from nine healthy volunteers who had received the two doses of BNT162b2 (Pfizer-BioNTech) vaccine (Table 1) and tested for neutralizing activity against the lentiviral reporters pseudotyped with the 14 L452 spike variants that showed expression and virion incorporation levels comparable to the WT D614G (Fig. 3A). Half of the L452 variants (7 of 14) maintained the sensitivity to the antisera with <20% difference in NT50. On the other hand, L452R and L452Q showed a >20% decrease in sensitivity (Fig. 4A), which in good agreement with previous studies demonstrating that L452 mutations play some roles in escape from neutralizing antibodies in epsilon, delta, and lambda variants (13, 16, 18, 24, 38). Interestingly, we found that the L452T mutant significantly (>60%) enhanced the sensitivity to neutralization by vaccine-induced antisera (Fig. 4A).

Next, we wanted to test the neutralization sensitivity when the naturally arising L452 mutations were introduced into BA.2 spike. In this assay, we used another panel of antisera from nine healthy volunteers who had received the three doses of BNT162b2 (Pfizer-BioNTech) or mRNA-1273 (Moderna) (Table 1) as BA.2 acquired substantial resistance against vaccinated antisera obtained from a two-dose regimen (39). No difference was observed in neutralization sensitivity between BA.2 spike and its L452 mutations to M, Q, and R (Fig. 4B), suggesting that none of the L452 mutations on the omicron BA.2 backbone was selected due to their reduced sensitivity to neutralization.

A nonamer peptide <sub>448</sub>-NYNYLYRLF<sub>-456</sub> (here "NF9"), which spans the spike L452 residue

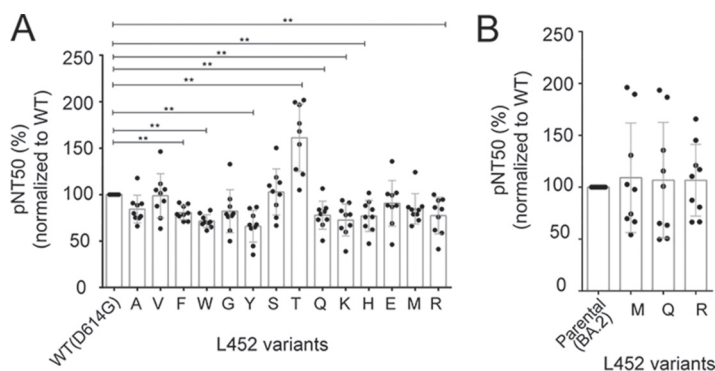


**FIG 4** Changes in neutralizing sensitivity by L452 spike variants. (A and B) Neutralizing sensitivity expressed as the pseudovirus neutralizing titer (pNT50) of sera from nine donors receiving two and three doses of the vaccines (Table 1) against a panel of lentiviruses pseudotyped with L452 spike mutants in the context of WT D614G (A) and omicron BA.2 (B), respectively. The relative pNT50 (%) values normalized to their parental pairs are shown. The data shown are means  $\pm$  the SD of triplicate determinations. Statistical significance was determined by Wilcoxon paired signed rank test (\*,  $P < 0.05$ ; \*\*,  $P < 0.01$ ).

at its fifth position, is an immunodominant CTL epitope presented by HLA-A\*24:02, a prevalent HLA allele in Asia (20–22, 40), and the spike L452R mutation confers escape from recognition by the cognate CTLs (23). Three NF9-specific TCR clones were isolated from three donors (23) and determined their TCR gene usages (Table 2). TCR clonotypes were found to be very similar. Specifically, in the TCR  $\alpha$  chain, the identical V segment was shared by T1 and T3, and the same J segment was shared by T1 and T2. In the TCR  $\beta$  chain, all harbored the same J segment and only one amino acid difference at the complementary determining region 3 (CDR3) (Table 2). To analyze their reactivity toward the panel of NF9 and NF9\_5X peptide (where “X” represents any amino acid substitution at the fifth position of the peptide), we used previously established reporter T cell assay (41). The A549 cells expressing HLA-A\*24:02 as target cells were pulsed with a set of the synthetic peptides, followed by co-culture with Jurkat cells expressing the cognate TCRs as effector cells (Fig. 5A). As expected from similar TCR clonotypes (Table 2), all three TCRs showed very similar cross-reactivity profiles (Fig. 5B). Specifically, all TCRs recognized variant peptides NF9\_5V, 5I and 5T comparably to NF9, and peptide NF9\_5W to a lesser extent. In contrast, while TCR 1 and TCR 3 showed minimal cross-reactivity to the peptide NF9\_5N and 5M, TCR 2 showed none. No TCR could cross-recognize the other 13 variant peptides (Fig. 5B). Furthermore, we examined the TCR cross-reactivity of L452 variants in the context of the omicron BA.2 spike. DNAs encoding the omicron BA.2 spike and its L452-M, -Q, and -R mutants were transfected to HLA-A\*24:02-expressing A542 cells and tested for recognition by the same TCRs (Fig. 5A). The results showed that none of the naturally arising L452 variants (i.e., L452-M, -Q and -R) retained sensitivity to TCR recognition (Fig. 5C). Of interest, the L452T mutant, which is naturally absent, showed greater sensitivity to neutralization by antisera and TCRs isolated from vaccine recipients (Fig. 4A and 5B).

**TABLE 2** Clonotypes of NF9-specific TCRs

TCR	Donor ID	TRA <sup>a</sup>			TRB <sup>b</sup>			
		V <sup>c</sup>	J <sup>d</sup>	CDR3 <sup>e</sup>	V	J	D <sup>f</sup>	CDR3
T1	GV34#3-4	TRAV12-1*01	TRAJ33*01	CVVNLFDSDNYQLIW	TRBV2*01	TRBJ2-7*01	TRBD1*01	CASSEGAGYEQYF
T2	GV36#16-2	TRAV12-2*02	TRAJ33*01	CAVNLKDSNYQLIW	TRBV6-1*01	TRBJ2-7*01	TRBD2*01	CASSEGGYEQYF
T3	KK08#14-1	TRAV12-1*01	TRAJ12*01	CVVNIIMDSYKLIIF	TRBV6-4*01	TRBJ2-7*01	TRBD2*02	CASSEGEGYEQYF

<sup>a</sup>TRA, T cell receptor alpha chain.

<sup>b</sup>TRB, T cell receptor beta chain.

<sup>c</sup>V, V segment.

<sup>d</sup>J, J segment.

<sup>e</sup>CDR3, complementary determining region 3.

<sup>f</sup>D, D segment.

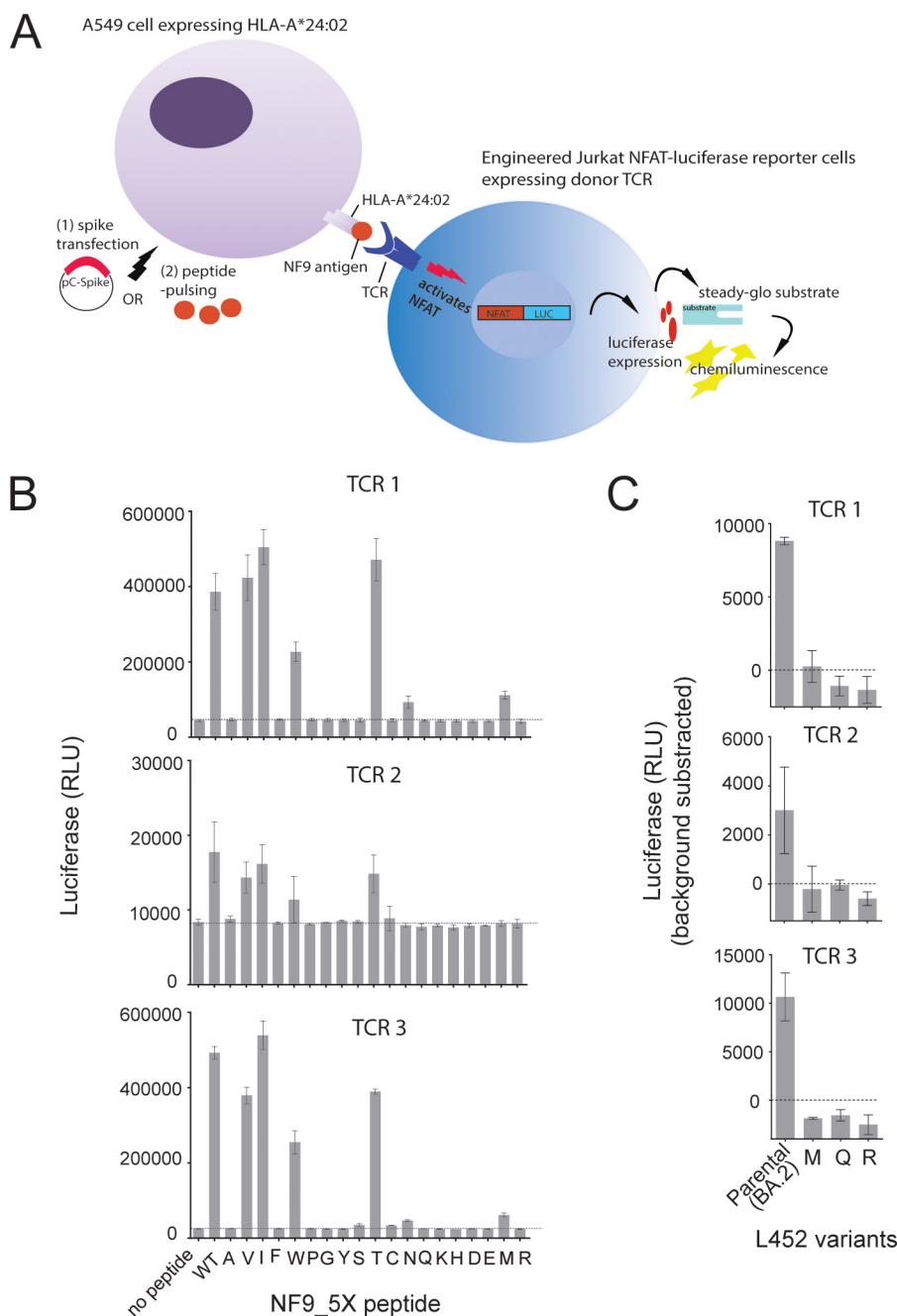


**FIG 5** Changes in TCR recognition by L452 spike variants. (A) Schematic diagram of TCR recognition assay. NFAT-luciferase Jurkat T reporter cells ( $TCR\alpha\beta^{-/-}$ ) expressing the defined  $\alpha\beta$  TCR clonotypes were used as effector cells. A549 cells expressing human ACE2 receptor and HLA-A\*24:02 (A549/hACE2/HLA-A\*24:02) were loaded with a panel of synthetic peptides or transfected with a panel of genes expressing spike proteins and used as target cells. (B and C) TCR activation level as measured by luciferase activity. A549/hACE2/HLA-A\*24:02 target cells loaded with a panel of NF9 and the indicated mutant peptides (B) and transfected by DNAs encoding BA.2 spike and its L452 variants (C) were cocultured with the NFAT-luciferase Jurkat T reporter cells that had been engineered to stably express the indicated NF9-specific TCR clones. The data shown are means  $\pm$  the SD of triplicate determinations.

**DISCUSSION**

In the present study, by employing a systematic and comprehensive analysis of recurrent mutations at SARS-CoV-2 spike L452, we demonstrated that the naturally arising L452 mutations in SARS-CoV-2 VOCs were characterized by (i) SNAM amino acid changes, (ii) amino acid residues that maintain a steady-state expression level and downstream



intracellular processing, (iii) enhancement of spike fusogenicity, (iv) enhancement of pseudovirus infectivity, and (v) amino acid mutations associated with less susceptibility to neutralization and TCR recognition.

Structural analysis shows that amino acids with longer and/or positively charged side chains at the position 452 tend to demonstrate better viral entry probably due to a steric clash with neighboring residues that leads to RBD up-conformation, which is known to be more accessible to the ACE2 receptor (37). Interestingly, glutamic acid (E) which contains a long side chain showed a rather modestly enhanced entry, probably due to additional restraint in conformation by its negative charge. Further detailed structural analysis is needed to elucidate the molecular basis of L452 mutations.

Of additional interest, the L452T mutant, which is naturally absent, showed greater sensitivity to neutralization by antisera and TCRs isolated from vaccine recipients. One could infer that the L452 mutation results in forming a classical N-x-S/T motif for N-linked glycosylation because the amino acid residue at position 450 was asparagine. The addition of glycan at N450 could influence the RBD conformation and sensitivity to immune recognition. However, such enhanced immune recognition was observed in L452T, but not in L452S. Whether the L452T mutant could be more immunogenic when introduced into vaccine platforms warrants further evaluation.

Our study employed a lentiviral pseudotyping system for the phenotypic analysis. It is important to note that the mutational effects of spike proteins on the infectivity of the authentic SARS-CoV-2 may have different profiles. Thus, further studies are needed to clarify this issue by creating recombinant SARS-CoV-2 particles harboring defined L452 mutations with reverse genetic technology, as demonstrated in a previous study (23). Despite this limitation, our findings suggest that the codon base change mutational barrier is a prerequisite for amino acid substitutions at L452, in addition to the phenotypic advantages of viral fitness and decreased sensitivity to host immunity, highlighting a convergent evolutionary pathway of SARS-CoV-2 spike protein in emerging variants.

## MATERIALS AND METHODS

**Phylogenetic analysis.** A maximum-likelihood phylogenetic tree of the coding regions (266 to 29,674 nucleotides [nt] in the reference sequence, EPI\_ISL\_402124) of the representative SARS-CoV-2 genomes was constructed. First, publicly available SARS-CoV-2 genome sequences (approximately 10.5 million) were downloaded from the GISAID EpiCoV database on 27 April 2022 (<https://www.gisaid.org/>). Sequences were excluded if (i) they carried any ambiguous bases (i.e., genetic codes other than A, U, G, and C) or (ii) they were shorter than 29,000 nt, as previously described (42). Next, the coding region of each filtered sequence was extracted, and a genotype was estimated by using a set of existing nucleotide mutations for the respective coding sequence, as previously described (42). A total of 25,796 major genotypes shared among  $\geq 10$  sequences (except recombinant lineages) were selected, and one sequence for each major genotype was applied for the phylogenetic analysis. Of note, no genotypes within the BA.4 lineage were shared among  $\geq 10$  sequences at the time of analysis. An approximate maximum-likelihood phylogenetic tree was constructed using FastTree (v2.1.11) with the GTR+CAT model (43). The tree was drawn using FigTree (v1.4.4; <http://tree.bio.ed.ac.uk/software/figtree/>). Selected sequences were also examined to detect amino acid mutations at spike position 452.

**Probability estimation model.** The probability of occurrences for each canonical amino acid substitution at position L452 was estimated by the number of nucleotide substitutions required for nonsynonymous mutation, together with the codonicity of each amino acid (i.e., the number of codons available for a particular amino acid). Substitution of one nucleotide (A/U/G/C) in a codon is computed at a probability of 0.25, two simultaneous nucleotides change at a probability of  $0.25^2$  and three simultaneous nucleotides change at a probability of  $0.25^3$ . In the event of amino acid substitution of leucine-452 (original codon CUG, as in ancestral SARS-CoV-2; GenBank [MN908947.3](https://www.ncbi.nlm.nih.gov/nuccore/MN908947.3)) by each of the canonical amino acids, the final probability of the event was calculated by adding up the nucleotide change probabilities of each codon coded for that particular amino acid.

**Plasmid constructs.** The firefly luciferase-expressing lentiviral transfer plasmid pWPI-Luc2, the HiBIT-tagged lentiviral packaging plasmid pSPAX2-IN/HiBIT, the ACE2-expressing plasmid pC-ACE2, the TMPRSS2-expressing plasmid pC-TMPRSS2, and the SARS-CoV-2 spike D614G-expressing plasmid pC-SARS2-S-D614G (generous gifts from Kenzo Tokunaga) have previously been described elsewhere (33). The SARS-CoV-2 spike L452 mutants in which the position L452 was mutated from leucine to other canonical amino acids, including alanine (L452A), valine (L452V), isoleucine (L452I), phenylalanine (L452F), tryptophan (L452W), proline (L452P), glycine (L452G), tyrosine (L452Y), serine (L452S), threonine (L452T), cysteine (L452C), asparagine (L452N), glutamine (L452Q), lysine (L452K), histidine (L452H), aspartic acid (L452D), glutamic acid (L452E),

methionine (L452M), and arginine (L452R) were prepared by PCR-based site-directed mutagenesis using pC-SARS-S-D614G as a template. The BA.2 L452 variants, including pC-SARS-S-BA.2-L452M, pC-SARS-S-BA.2-L452Q, and pC-SARS-S-BA.2-L452R, were constructed using pC-SARS2-S-BA.2 (39) (a generous gift from Kei Sato) as a template. The resultant PCR fragment was digested with KpnI and NotI and inserted into the corresponding site of the pCAGGS mammalian expression vector (44). Nucleotide sequences of the spike were determined by Genetic Analyzer 3500xL (Applied Biosystems), followed by analysis using GENETYX software (v12 622; GENETYX Corporation).

**Pseudovirus assay.** SARS-CoV-2 pseudoviruses were prepared by cotransfecting 1  $\mu$ g of pWPI-LUC2, 1  $\mu$ g of psPAX2-IN/HiBIT, and 400 ng of various spike-encoding plasmids in 293T cells ( $6 \times 10^5$ ) by using a polyethylenimine (PEI) Max transfection system (Polysciences, Inc., catalog no. 24765-1). The secreted viral particles were harvested from the culture supernatant, clarified by centrifugation at  $3,000 \times g$  for 3 min at 4°C, and quantified as assessed by NanoLuc expression that was proportional to the level of the p24 antigen, as described previously (45). To prepare 293T/ACE2/TMPRSS2-expressing target cells, equal amounts (500 ng) of pC-ACE2 and pC-TMPRSS2 were cotransfected in 293T cells ( $6 \times 10^5$ ). After 48 h, the cells were split and seeded at  $2.2 \times 10^4$  per well on a 96-well plate and then exposed to equal amounts of viral inoculum at titers of 1, 3, and 5 ng of the p24 antigen level. The single-round infectivity was determined 48 h later by measuring the luciferase activity with a One-Glo luciferase assay system (Promega, catalog no. E6130) in a Centro XS3 LB960 luminometer (Berthold Technologies). Data were normalized to WT D614G (5 ng) or parental BA.2 as 100%.

**Cell-to-cell fusion assay.** The SARS-CoV-2 spike-based fusion assay was performed based on a dual-split protein (DSP), DSP1-7 and DSP8-11, which together encode a chimera of *Renilla* luciferase (RL) and GFP reporter proteins (46, 47). To prepare spike-expressing cells, HEK293T cells ( $3 \times 10^5$ ) seeded on a 24-well plate were cotransfected with equal amounts (200 ng) of pDSP1-7 and various spike-expressing plasmids, as indicated above. To prepare ACE2- and TMPRSS2-expressing target cells, HEK293 cells ( $8 \times 10^5$ ) seeded on a six-well plates were cotransfected with 500 ng of pC-ACE2, 250 ng of pC-TMPRSS2, and 500 ng of pDSP8-11. At 48 h posttransfection, the ACE2- and TMPRSS2-expressing cells were incubated with EnduRen live cell substrate (Promega, catalog no. E6481) for 3 h. Then, the spike-expressing cells ( $1.6 \times 10^4$  per well) and ACE2- and TMPRSS2-expressing cells ( $3.2 \times 10^4$  per well) were mixed in a 96-well black plate (Falcon, catalog no. 353376), and the RL activity was measured at the indicated time points by using a Centro XS3 LB960 luminometer (Berthold Technologies).

**Protein structure.** The cryo-electron microscopy structure of a full-length spike trimer (PDB 7KRR) (36) was drawn using PyMOL v2.3 (<https://pymol.org/2/>).

**Western blotting.** The samples for immunoblotting were prepared as described previously (48). Briefly, transfected cells were lysed directly on ice for 15 min in a buffer (100 mM NaCl, 1 mM TCEP [Tris (2-carboxyethyl)phosphine hydrochloride], 2 $\times$  protease inhibitor, and 10 mM HEPES; pH 7.5) containing 1% *n*-dodecyl- $\beta$ -D-maltoside (DDM; Nacalai Tesque, catalog no. 14239-41). For the spike incorporation study, the virus-containing culture supernatant was clarified by filtering through a 0.45- $\mu$ m-pore-size filter, layered onto a 20% (wt/vol) sucrose cushion, pelleted by ultracentrifugation at 50,000 rpm for 30 min at 4°C (Beckman Coulter Optima-TLX), and then lysed in 1% DDM buffer. The resultant samples were resuspended in 1 $\times$  Laemmli buffer containing 5%  $\beta$ -mercaptoethanol (Bio-Rad, catalog no. 1610710), boiled for 10 min, and subjected to protein separation by SDS-PAGE in 4 to 20% Mini-Protean TGX precast gels (Bio-Rad, catalog no. 4561096) before transfer to nitrocellulose membranes (Wako, catalog no. 032-22663). The membranes were incubated in a blocking buffer (Nacalai Tesque, catalog no. 03953-95) for 1 h at room temperature and then mixed with primary antibodies, including mouse anti-SARS-CoV-2 Spike (S2 subunit) monoclonal antibody (1:4,000; GeneTex, catalog no. GTX632604), rabbit anti-HIV Gag p24 monoclonal antibody (1:5,000; Bioacademia, catalog no. 65-004), and mouse anti- $\beta$ -actin monoclonal antibody (1:5,000; Wako, catalog no. 281-98721), followed by staining with the appropriate secondary antibodies, horseradish peroxidase-conjugated anti-mouse (1:25,000; GE Healthcare, catalog no. NA931VS) or anti-rabbit (1:50,000; GE Healthcare, catalog no. NA94VS) IgG antibodies. The membrane was developed with the ImmunoStar LD enhanced chemiluminescence reagents (Wako, catalog no. 290-69904) and visualized using ImageQuant LAS 400 (GE Healthcare). Band intensities were analyzed using ImageJ software (49).

**Pseudovirus neutralization assay.** Serum samples were collected from nine donors with two doses of BNT162b2 (Pfizer-BioNTech) and another group of nine donors with three doses of vaccines, including BNT162b2 or mRNAQ-123 (Moderna) (Table 1). The serum samples were heat inactivated at 56°C for 30 min and stored at  $-80^\circ\text{C}$  until use. To compare the neutralizing activity against different spike-pseudotyped lentiviruses, 2-fold serially diluted sera were mixed with an equal volume of pseudoviruses (5 ng of p24 level per well) and incubated at 37°C for 1 h. Finally,  $2.2 \times 10^4$  293T cells transiently expressing ACE2 and TMPRSS2 were added into each well in a 96-well plate and incubated further for 48 h prior to quantification of luciferase expression using a One-Glo luciferase assay system in Centro XS3 LB960 luminometer (Berthold Technologies). The neutralization level was determined by the percent decrease in luminescence relative to that obtained in the absence of sera. Neutralization curves were plotted, and 50% pseudovirus neutralization titer (pNT50) values (in serum dilution factor) were inferred using GraphPad Prism, and expressed in percentage normalized to parental WT D614G or BA.2. Prepandemic sera isolated from three donors were simultaneously tested and always yielded negative results for neutralization.

**T cell receptor recognition assay.** Construction of NF9-specific effector T cells and TCR activation assays were performed as previously described (23, 41, 50). In brief, TCR clones were reconstituted and stably expressed in an NFAT-luciferase Jurkat T reporter cell line (TCR $\alpha\beta$ <sup>-/-</sup>) that allows detection of T cell activation. Also, HLA-A\*24:02 was stably transduced in A549-expressing human ACE2 receptor, giving rise to A549/hACE2/HLA-A\*24:02 (23, 50). A549/hACE2/HLA-A\*24:02 target cells were loaded with no

peptide or a panel of NF9 and NF9\_5X peptides (where “X” represents any amino acid substitution at the fifth position of the peptide) in a final concentration of 50 nM. Alternatively, the same target cells were transfected or not with 2  $\mu$ g of various spike-expressing plasmids, pC-BA.2, pC-BA.2-L452M, pC-BA.2-L452Q, and pC-BA.2-L452R for 48 h. In both cases, target cells ( $0.5 \times 10^5$  per well) and NFAT-luciferase Jurkat T reporter cells expressing NF9-specific TCR clones ( $1 \times 10^5$  per well) were cocultured in a 96-well plate for 8 h. The T cell activation level was measured by detecting the luciferase activity using a Steady-Glo assay system (Promega, catalog no. E2550) in a Centro XS3 LB960 luminometer.

**Statistical analysis.** Statistical tests were performed by using GraphPad Prism 6. Standard deviations (SD) were calculated to estimate the variance. Statistical comparisons were made as described for each data set and figure. A *P* value of <0.05 was considered significant.

## ACKNOWLEDGMENTS

We thank Kenzo Tokunaga (National Institute of Infectious Disease, Tokyo, Japan) and Kei Sato and Jin Gohda (University of Tokyo, Tokyo, Japan) for providing the necessary reagents.

This study was supported in part by AMED Research Program on Emerging and Re-emerging Infectious Diseases 20fk0108539h0001 and 20fk0108451s0101 (to T.U.) and AMED Research Program on HIV/AIDS 21fk0410046 (to C.M.), JSPS KAKENHI Grants-in-Aid for Scientific Research B 19H03703 and 22H03119 (to T.U.) and 22H02877 (to C.M.), Scientific Research C grants 19K07623 (to C.M.) and 22K07089 (to M.T.), Takeda Science Foundation grants (to C.M. and M.T.) and an intramural grant from Kumamoto University COVID-19 Research Projects (AMABIE) (to C.M.), IMAI Memorial Trust for AIDS Research (to M.T.), and Shin-Nihon Foundation of Advanced Medical Research (to M.T.). This study was also supported in part by JSPS Bilateral Open Partnership Joint Research Project, JPJSBP120219933 and JSPS Core-to-Core Program, JPJSCCB20220010 (to T.U.).

The authors declare there are no competing interests.

Conceptualization: T.S.T., M.T., C.M., and T.U.; reagents and specimens: M.T., G.B., H.H., M.K., H.K., and C.M.; data collection: T.S.T., M.T., H.O., C.M., and Y.I.; manuscript writing: T.S.T. and T.U.; supervision: T.U.; funding acquisition: M.T., C.M., and T.U.

## REFERENCES

- Lan J, Ge J, Yu J, Shan S, Zhou H, Fan S, Zhang Q, Shi X, Wang Q, Zhang L, Wang X. 2020. Structure of the SARS-CoV-2 spike receptor-binding domain bound to the ACE2 receptor. *Nature* 581:215–220. <https://doi.org/10.1038/s41586-020-2180-5>.
- Iacobucci G. 2021. Covid-19: New UK variant may be linked to increased death rate, early data indicate. *BMJ* 372:n230. <https://doi.org/10.1136/bmj.n230>.
- Tegally H, Wilkinson E, Giovanetti M, Iranzadeh A, Fonseca V, Giandhari J, Doolabh D, Pillay S, San EJ, Msomi N, Mlisana K, von Gottberg A, Walaza S, Allam M, Ismail A, Mohale T, Glass AJ, Engelbrecht S, Van Zyl G, Preiser W, Petruccione F, Sigal A, Hardie D, Marais G, Hsiao NY, Korsman S, Davies MA, Tyers L, Mudau I, York D, Maslo C, Goedhals D, Abrahams S, Laguda-Akingba O, Alisoltani-Dehkordi A, Godzik A, Wibmer CK, Sewell BT, Lourenço J, Alcantara LCJ, Kosakovsky Pond SL, Weaver S, Martin D, Lessells RJ, Bhiman JN, Williamson C, de Oliveira T. 2021. Detection of a SARS-CoV-2 variant of concern in South Africa. *Nature* 592:438–443. <https://doi.org/10.1038/s41586-021-03402-9>.
- Voloch CM, Silva F, de Almeida LGP, Cardoso CC, Brustolini OJ, Gerber AL, Guimarães A, Mariani D, Costa R, Ferreira OC, Cavalcanti AC, Frauches TS, de Mello CMB, Galliez RM, Faffe DS, Castiñeiras TMPP, Tanuri A, de Vasconcelos ATR. 2020. Genomic characterization of a novel SARS-CoV-2 lineage from Rio de Janeiro, Brazil. *medRxiv*. <https://www.medrxiv.org/content/10.1101/2020.12.23.20248598v1>.
- Mlcochova P, Kemp SA, Dhar MS, Papa G, Meng B, Ferreira IATM, Datir R, Collier DA, Albecka A, Singh S, Pandey R, Brown J, Zhou J, Goonawardane N, Mishra S, Whittaker C, Mellan T, Marwal R, Datta M, Sengupta S, Ponnusamy K, Radhakrishnan VS, Abdullahi A, Charles O, Chattopadhyay P, Devi P, Caputo D, Peacock T, Wattal C, Goel N, Satwik A, Vaishya R, Agarwal M, Mavousian A, Lee JH, Bassi J, Silacci-Fegni C, Saliba C, Pinto D, Irie T, Yoshida I, Hamilton WL, Sato K, Bhatt S, Flaxman S, James LC, Corti D, Piccoli L, Barclay WS, Rakshit P, CITIID-NIHR BioResource COVID-19 Collaboration, et al. 2021. SARS-CoV-2 B.1.617.2 delta variant replication and immune evasion. *Nature* 599:114–119. <https://doi.org/10.1038/s41586-021-03944-y>.
- Meng B, Abdullahi A, Ferreira IATM, Goonawardane N, Saito A, Kimura I, Yamasoba D, Gerber PP, Fathi S, Rathore S, Zepeda SK, Papa G, Kemp SA, Ikeda T, Toyoda M, Tan TS, Kuramochi J, Mitsunaga S, Ueno T, Shirakawa K, Takaori-Kondo A, Brevini T, Mallery DL, Charles OJ, Baker S, Dougan G, Hess C, Kingston N, Lehner PJ, Lyons PA, Matheson NJ, Ouwehand WH, Saunders C, Summers C, Thaventhiran JED, Toshner M, Weekes MP, Maxwell P, Shaw A, Bucke A, Calder J, Canna L, Domingo J, Elmer A, Fuller S, Harris J, Hewitt S, Kennet J, Jose S, Kourampa J, The CITIID-NIHR BioResource COVID-19 Collaboration, et al. 2022. Altered TMPRSS2 usage by SARS-CoV-2 omicron impacts tropism and fusogenicity. *Nature* 603:706–714. <https://doi.org/10.1038/s41586-022-04474-x>.
- Tchesnokova V, Kulasekara H, Larson L, Bowers V, Rechkina E, Kisiela D, Sledneva Y, Choudhury D, Maslova I, Deng K, Kutumbaka K, Geng H, Fowler C, Greene D, Ralston J, Samadpour M, Sokurenko E. 2021. Acquisition of the L452R mutation in the ACE2-binding interface of Spike protein triggers recent massive expansion of SARS-CoV-2 variants. *J Clin Microbiol* 59:e00921-21. <https://doi.org/10.1128/JCM.00921-21>.
- Deng X, Garcia-Knight MA, Khalid MM, Servellita V, Wang C, Morris MK, Sotomayor-González A, Glasner DR, Reyes KR, Gliwa AS, Reddy NP, Sanchez San Martin C, Federman S, Cheng J, Balcerak J, Taylor J, Streithorst JA, Miller S, Sreekumar B, Chen P-Y, Schulze-Gahmen U, Taha TY, Hayashi JM, Simoneau CR, Kumar GR, McMahon S, Lidsky PV, Xiao Y, Hemarajata P, Green NM, Espinosa A, Kath C, Haw M, Bell J, Hacker JK, Hanson C, Wadford DA, Anaya C, Ferguson D, Frankino PA, Shivram H, Lareau LF, Wyman SK, Ott M, Andino R, Chiu CY. 2021. Transmission, infectivity, and neutralization of a spike L452R SARS-CoV-2 variant. *Cell* 184:3426–3437.e8. <https://doi.org/10.1016/j.cell.2021.04.025>.
- Zhang W, Davis BD, Chen SS, Sincuir Martinez JM, Plummer JT, Vail E. 2021. Emergence of a novel SARS-CoV-2 variant in southern California. *JAMA* 325:1324–1326. <https://doi.org/10.1001/jama.2021.1612>.
- Lu L, Sikkema RS, Velkers FC, Nieuwenhuijse DF, Fischer EAJ, Meijer PA, Bouwmeester-Vincken N, Rietveld A, Wegdam-Blans MCA, Tolsma P, Koppelman M, Smit LAM, Hakze-van der Honing RW, van der Poel WHM, van der Spek AN, Spierenburg MAH, Molenaar RJ, Rond J, Augustijn M,

Woolhouse M, Stegeman JA, Lycett S, Oude Munnink BB, Koopmans MPG. 2021. Adaptation, spread and transmission of SARS-CoV-2 in farmed minks and associated humans in the Netherlands. *Nat Commun* 12:6802. <https://doi.org/10.1038/s41467-021-27096-9>.

11. Munnink BBO, Sikkema RS, Nieuwenhuijse DF, Molenaar RJ, Munger E, Molenkamp R, Spek A, Tolsma P, Rietveld A, Brouwer M, Bouwmeester-Vincken N, Harders F, Honing RH-v, Wegdam-Blans MCA, Bouwstra RJ, GeurtsvanKessel C, Eijk A, Velkers FC, Smit LAM, Stegeman A, Poel W, Koopmans MPG. 2021. Transmission of SARS-CoV-2 on mink farms between humans and mink and back to humans. *Science* 371:172–177. <https://doi.org/10.1126/science.abe5901>.
12. Hoffmann M, Zhang L, Krüger N, Graichen L, Kleine-Weber H, Hofmann-Winkler H, Kempf A, Nessler S, Riggert J, Winkler MS, Schulz S, Jäck HM, Pöhlmann S. 2021. SARS-CoV-2 mutations acquired in mink reduce antibody-mediated neutralization. *Cell Rep* 35:109017. <https://doi.org/10.1016/j.celrep.2021.109017>.
13. Kimura I, Kosugi Y, Wu J, Zahradnik J, Yamasoba D, Butlertanaka EP, Tanaka YL, Uriu K, Liu Y, Morizako N, Shirakawa K, Kazuma Y, Nomura R, Horisawa Y, Tokunaga K, Ueno T, Takaori-Kondo A, Schreiber G, Arase H, Motozono C, Saito A, Nakagawa S, Sato K. 2022. The SARS-CoV-2 lambda variant exhibits enhanced infectivity and immune resistance. *Cell Rep* 38:110218. <https://doi.org/10.1016/j.celrep.2021.110218>.
14. McCallum M, Walls AC, Sprouse KR, Bowen JE, Rosen LE, Dang HV, Marco AD, Franko N, Tilles SW, Logue J, Miranda MC, Ahlrichs M, Carter L, Snell G, Pizzuto MS, Chu HY, Voorhis WCV, Corti D, Veelsler D. 2021. Molecular basis of immune evasion by the delta and kappa SARS-CoV-2 variants. *Science* 374:1621–1626. <https://doi.org/10.1126/science.abc8506>.
15. Kaleta T, Kern L, Hong SL, Hölzer M, Kochs G, Beer J, Schnepf D, Schwemmler M, Bollen N, Kolb P, Huber M, Ulferts S, Weigang S, Dudas G, Wittig A, Jaki L, Padane A, Lagare A, Salou M, Ozer EA, Nnaemeka N, Odoom JK, Rutayisire R, Benkahla A, Akoua-Koffi C, Ouedraogo A-S, Simon-Lorière E, Enouf V, Kröger S, Calvignac-Spencer S, Baele G, Panning M, Fuchs J. 2022. Antibody escape and global spread of SARS-CoV-2 lineage A.27. *Nat Commun* 13:1152. <https://doi.org/10.1038/s41467-022-28766-y>.
16. Planas D, Veyer D, Baidaliuk A, Staropoli I, Guivel-Benhassine F, Rajah MM, Planchais C, Porrot F, Robillard N, Puech J, Prot M, Gallais F, Gantner P, Velay A, Le Guen J, Kassis-Chikhani N, Edriss D, Belec L, Seve A, Courtellemont L, Péré H, Hocqueloux L, Fafi-Kremer S, Prazuck T, Mouquet H, Bruel T, Simon-Lorière E, Rey FA, Schwartz O. 2021. Reduced sensitivity of SARS-CoV-2 variant Delta to antibody neutralization. *Nature* 596:276–280. <https://doi.org/10.1038/s41586-021-03777-9>.
17. Shen X, Tang H, Pajon R, Smith G, Glenn GM, Shi W, Korber B, Montefiori DC. 2021. Neutralization of SARS-CoV-2 variants B.1.429 and B.1.351. *N Engl J Med* 384:2352–2354. <https://doi.org/10.1056/NEJMc2103740>.
18. Tada T, Zhou H, Dcosta BM, Samanovic MI, Mulligan MJ, Landau NR. 2021. Partial resistance of SARS-CoV-2 Delta variants to vaccine-elicited antibodies and convalescent sera. *iScience* 24:103341. <https://doi.org/10.1016/j.isci.2021.103341>.
19. Li Q, Wu J, Nie J, Zhang L, Hao H, Liu S, Zhao C, Zhang Q, Liu H, Nie L, Qin H, Wang M, Lu Q, Li X, Sun Q, Liu J, Zhang L, Li X, Huang W, Wang Y. 2020. The impact of mutations in SARS-CoV-2 spike on viral infectivity and antigenicity. *Cell* 182:1284–1294.e9. <https://doi.org/10.1016/j.cell.2020.07.012>.
20. Gao A, Chen Z, Amitai A, Doelger J, Mallajosyula V, Sundquist E, Pereyra Segal F, Carrington M, Davis MM, Streeck H, Chakraborty AK, Julg B. 2021. Learning from HIV-1 to predict the immunogenicity of T cell epitopes in SARS-CoV-2. *iScience* 24:102311. <https://doi.org/10.1016/j.isci.2021.102311>.
21. Kared H, Redd AD, Bloch EM, Bonny TS, Sumatoh H, Kairi F, Carbajo D, Abel B, Newell EW, Bettinotti MP, Benner SE, Patel EU, Littlefield K, Laeyendecker O, Shoham S, Sullivan D, Casadevall A, Pekosz A, Nardin A, Fehlings M, Tobian AA, Quinn TC. 2021. SARS-CoV-2-specific CD8<sup>+</sup> T cell responses in convalescent COVID-19 individuals. *J Clin Invest* 131:e145476. <https://doi.org/10.1172/JCI145476>.
22. Hu C, Shen M, Han X, Chen Q, Li L, Chen S, Zhang J, Gao F, Wang W, Wang Y, Li T, Li S, Huang J, Wang J, Zhu J, Chen D, Wu Q, Tao K, Pang D, Jin A. 2022. Identification of cross-reactive CD8<sup>+</sup> T cell receptors with high functional avidity to a SARS-CoV-2 immunodominant epitope and its natural mutant variants. *Genes Dis* 9:216–229. <https://doi.org/10.1016/j.gendis.2021.05.006>.
23. Motozono C, Toyoda M, Zahradnik J, Saito A, Nasser H, Tan TS, Ngare I, Kimura I, Uriu K, Kosugi Y, Yue Y, Shimizu R, Ito J, Torii S, Yonekawa A, Shimono N, Nagasaki Y, Minami R, Toya T, Sekiya N, Fukuhara T, Matsuura Y, Schreiber G, Ikeda T, Nakagawa S, Ueno T, Sato K, Genotype to Phenotype Japan (G2P-Japan) Consortium. 2021. SARS-CoV-2 spike L452R variant evades cellular immunity and increases infectivity. *Cell Host Microbe* 29:1124–1136.e11. <https://doi.org/10.1016/j.chom.2021.06.006>.
24. Zhou Z, Du P, Yu M, Baptista-Hon DT, Miao M, Xiang AP, Lau JY-N, Li N, Xiong X, Huang H, Liu Z, Dai Q, Zhu J, Wu S, Li G, Zhang K, Group C-II, COVID-19 Immunity Investigation Group. 2021. Assessment of infectivity and the impact on neutralizing activity of immune sera of the COVID-19 variant, CAL.20C. *Signal Transduction and Targeted Therapy* 6:285. <https://doi.org/10.1038/s41392-021-00695-0>.
25. Vargas-Herrera N, Araujo-Castillo RV, Mestanza O, Galarza M, Rojas-Serrano N, Solari-Zerpa L. 2022. SARS-CoV-2 Lambda and Gamma variants competition in Peru, a country with high seroprevalence. *Lancet Reg Health Am* 6:100112. <https://doi.org/10.1016/j.lana.2021.100112>.
26. World Health Organization. 2022. Tracking SARS-CoV-2 variants. World Health Organization, Geneva, Switzerland.
27. Cao Y, Yisimayi A, Jian F, Song W, Xiao T, Wang L, Du S, Wang J, Li Q, Chen X, Wang P, Zhang Z, Liu P, An R, Hao X, Wang Y, Feng R, Sun H, Zhao L, Zhang W, Zhao D, Zheng J, Yu L, Li C, Zhang N, Wang R, Niu X, Yang S, Song X, Zheng L, Li Z, Gu Q, Shao F, Huang W, Jin R, Shen Z, Wang Y, Wang X, Xiao J, Xie XS. 2022. BA.2.12.1, BA.4 and BA.5 escape antibodies elicited by Omicron infection. *bioRxiv*. <https://www.biorxiv.org/content/10.1101/2022.04.30.489997v2>.
28. Hou W. 2020. Characterization of codon usage pattern in SARS-CoV-2. *Virology* 541:173–188. <https://doi.org/10.1016/j.virus.2020.07.013>.
29. Balasco N, Damaggio G, Esposito L, Villani F, Berisio R, Colonna V, Vitagliano L. 2021. A global analysis of conservative and non-conservative mutations in SARS-CoV-2 detected in the first year of the COVID-19 world-wide diffusion. *Sci Rep* 11:24495. <https://doi.org/10.1038/s41598-021-04147-1>.
30. Morgan AA, Rubenstein E. 2013. Proline: the distribution, frequency, positioning, and common functional roles of proline and polyproline sequences in the human proteome. *PLoS One* 8:e53785. <https://doi.org/10.1371/journal.pone.0053785>.
31. Wedemeyer WJ, Welker E, Narayan M, Scheraga HA. 2000. Disulfide bonds and protein folding. *Biochemistry* 39:4207–4216. <https://doi.org/10.1021/bi992922o>.
32. Bass J, Turck C, Rouard M, Steiner DF. 2000. Furin-mediated processing in the early secretory pathway: sequential cleavage and degradation of misfolded insulin receptors. *Proc Natl Acad Sci U S A* 97:11905–11909. <https://doi.org/10.1073/pnas.97.22.11905>.
33. Ozono S, Zhang Y, Ode H, Sano K, Tan TS, Imai K, Miyoshi K, Kishigami S, Ueno T, Iwatani Y, Suzuki T, Tokunaga K. 2021. SARS-CoV-2 D614G spike mutation increases entry efficiency with enhanced ACE2-binding affinity. *Nat Commun* 12:848. <https://doi.org/10.1038/s41467-021-21118-2>.
34. Pal D. 2021. Spike protein fusion loop controls SARS-CoV-2 fusogenicity and infectivity. *J Struct Biol* 213:107713. <https://doi.org/10.1016/j.jsb.2021.107713>.
35. Teeranaipong P, Hosoya N, Kawana-Tachikawa A, Fujii T, Koibuchi T, Nakamura H, Koga M, Kondo N, Gao GF, Hoshino H, Matsuda Z, Iwamoto A. 2013. Development of a rapid cell-fusion-based phenotypic HIV-1 tropism assay. *J Int AIDS Soc* 16:18723–18723. <https://doi.org/10.7448/IAS.16.1.18723>.
36. Zhang J, Cai Y, Xiao T, Lu J, Peng H, Sterling SM, Walsh RM, Rits-Volloch S, Zhu H, Woosley AN, Yang W, Sliz P, Chen B. 2021. Structural impact on SARS-CoV-2 spike protein by D614G substitution. *Science* 372:525–530. <https://doi.org/10.1126/science.abc2303>.
37. Wang Y, Liu C, Zhang C, Wang Y, Hong Q, Xu S, Li Z, Yang Y, Huang Z, Cong Y. 2022. Structural basis for SARS-CoV-2 Delta variant recognition of ACE2 receptor and broadly neutralizing antibodies. *Nat Commun* 13:871. <https://doi.org/10.1038/s41467-022-28528-w>.
38. Wang M, Zhang L, Li Q, Wang B, Liang Z, Sun Y, Nie J, Wu J, Su X, Qu X, Y L, Wang Y, Huang W. 2022. Reduced sensitivity of the SARS-CoV-2 Lambda variant to monoclonal antibodies and neutralizing antibodies induced by infection and vaccination. *Emerg Microbes Infect* 11:18–29. <https://doi.org/10.1080/22221751.2021.2008775>.
39. Yamasoba D, Kimura I, Nasser H, Morioka Y, Nao N, Ito J, Uriu K, Tsuda M, Zahradnik J, Shirakawa K, Suzuki R, Kishimoto M, Kosugi Y, Kobiyama K, Hara T, Toyoda M, Tanaka YL, Butlertanaka EP, Shimizu R, Ito H, Wang L, Oda Y, Orba Y, Sasaki M, Nagata K, Yoshimatsu K, Asakura H, Nagashima M, Sadamasu K, Yoshimura K, Kuramochi J, Seki M, Fujiki R, Kaneda A, Shimada T, Nakada T-a, Sakao S, Suzuki T, Ueno T, Takaori-Kondo A, Ishii KJ, Schreiber G, Sawa H, Saito A, Irie T, Tanaka S, Matsuno K, Fukuhara T, Ikeda T, Sato K. 2022. Virological characteristics of the SARS-CoV-2 Omicron BA.2 spike. *Cell* 185:2103–2115. <https://doi.org/10.1016/j.cell.2022.04.035>.



40. Kiyotani K, Toyoshima Y, Nemoto K, Nakamura Y. 2020. Bioinformatic prediction of potential T cell epitopes for SARS-Cov-2. *J Hum Genet* 65: 569–575. <https://doi.org/10.1038/s10038-020-0771-5>.
41. Mahiti M, Toyoda M, Jia X, Kuang XT, Mwimanzi F, Mwimanzi P, Walker BD, Xiong Y, Brumme ZL, Brockman MA, Ueno T. 2016. Relative Resistance of HLA-B to Downregulation by Naturally Occurring HIV-1 Nef Sequences. *mBio* 7:e01516-15–e01515. <https://doi.org/10.1128/mBio.01516-15>.
42. Ode H, Nakata Y, Nagashima M, Hayashi M, Yamazaki T, Asakura H, Suzuki J, Kubota M, Matsuoka K, Matsuda M, Mori M, Sugimoto A, Imahashi M, Yokomaku Y, Sadamasu K, Iwatani Y. 2022. Molecular epidemiological features of SARS-CoV-2 in Japan. *Virus Evol* 8:veac034. <https://doi.org/10.1093/ve/veac034>.
43. Price MN, Dehal PS, Arkin AP. 2010. FastTree 2: approximately maximum-likelihood trees for large alignments. *PLoS One* 5:e0009490. <https://doi.org/10.1371/journal.pone.0009490>.
44. Niwa H, Yamamura K, Miyazaki J. 1991. Efficient selection for high-expression transfectants with a novel eukaryotic vector. *Gene* 108:193–199. [https://doi.org/10.1016/0378-1119\(91\)90434-d](https://doi.org/10.1016/0378-1119(91)90434-d).
45. Ozono S, Zhang Y, Tobiome M, Kishigami S, Tokunaga K. 2020. Super-rapid quantitation of the production of HIV-1 harboring a luminescent peptide tag. *J Biol Chem* 295:13023–13030. <https://doi.org/10.1074/jbc.RA120.013887>.
46. Ikeda T, Symeonides M, Albin JS, Li M, Thali M, Harris RS. 2018. HIV-1 adaptation studies reveal a novel Env-mediated homeostasis mechanism for evading lethal hypermutation by APOBEC3G. *PLoS Pathog* 14:e1007010. <https://doi.org/10.1371/journal.ppat.1007010>.
47. Kondo N, Miyauchi K, Matsuda Z. 2011. Monitoring viral-mediated membrane fusion using fluorescent reporter methods. *Curr Protoc Cell Biol* Chapter 26:Unit 26.9. <https://doi.org/10.1002/0471143030.cb2609s50>.
48. Tan TS, Toyoda M, Tokunaga K, Ueno T. 2021. Aromatic side chain at position 412 of SERINC5 exerts restriction activity toward HIV-1 and other retroviruses. *J Virol* 95:e00634-21. <https://doi.org/10.1128/JVI.00634-21>.
49. Schneider CA, Rasband WS, Eliceiri KW. 2012. NIH Image to ImageJ: 25 years of image analysis. *Nat Methods* 9:671–675. <https://doi.org/10.1038/nmeth.2089>.
50. Motozono C, Toyoda M, Tan TS, Hamana H, Goto Y, Aritsu Y, Miyashita Y, Oshiumi H, Nakamura K, Okada S, Udaka K, Kitamatsu M, Kishi H, Ueno T. 2022. The SARS-CoV-2 Omicron BA.1 spike G446S mutation potentiates antiviral T-cell recognition. *Nat Commun* 13:5440. <https://doi.org/10.1038/s41467-022-33068-4>.